

Global phase diagram of a spin-orbit-coupled Kondo lattice model on the honeycomb lattice

Xin Li,^{1,2} Rong Yu,^{3,*} and Qimiao Si^{4,†}

¹*Beijing National Laboratory for Condensed Matter Physics and Institute of Physics, Chinese Academy of Sciences, Beijing 100190, China*

²*University of Chinese Academy of Sciences, Beijing 100049, China*

³*Department of Physics and Beijing Key Laboratory of Opto-electronic Functional Materials and Micro-nano Devices, Renmin University of China, Beijing 100872, China*

⁴*Department of Physics & Astronomy, Rice Center for Quantum Materials, Rice University, Houston, Texas 77005, USA*
(Dated: December 20, 2018)

Motivated by the growing interest in the novel quantum phases in materials with strong electron correlations and spin-orbit coupling, we study the interplay between the spin-orbit coupling, Kondo interaction, and magnetic frustration of a Kondo lattice model on a two-dimensional honeycomb lattice. We calculate the renormalized electronic structure and correlation functions at the saddle point based on a fermionic representation of the spin operators. We find a global phase diagram of the model at half-filling, which contains a variety of phases due to the competing interactions. In addition to a Kondo insulator, there is a topological insulator with valence bond solid correlations in the spin sector, and two antiferromagnetic phases. Due to a competition between the spin-orbit coupling and Kondo interaction, the direction of the magnetic moments in the antiferromagnetic phases can be either within or perpendicular to the lattice plane. The latter antiferromagnetic state is topologically nontrivial for moderate and strong spin-orbit couplings.

I. INTRODUCTION

Exploring novel quantum phases and the associated phase transitions in systems with strong electron correlations is a major subject of contemporary condensed matter physics.¹⁻³ In this context, heavy fermion (HF) compounds play a crucial role.³⁻⁶ In these materials, the coexisted itinerant electrons and local magnetic moments (from localized f electrons) interact via the antiferromagnetic exchange coupling, resulting in the Kondo effect.⁷ Meanwhile, the Ruderman-Kittel-Kasuya-Yosida (RKKY) interaction, namely the exchange coupling among the local moments mediated by the itinerant electrons, competes with the Kondo effect.⁸ This competition gives rise to a rich phase diagram with an antiferromagnetic (AFM) quantum critical point (QCP) and various emergent phases nearby.^{3,9}

In the HF metals, experiments^{10,11} have provide strong evidence for local quantum criticality,^{12,13} which is characterized by the beyond-Landau physics of Kondo destruction at the AFM QCP. Across this local QCP, the Fermi surface jumps from large in the paramagnetic HF liquid phase to small in the AFM phase with Kondo destruction. A natural question is how this local QCP connects to the conventional spin density wave (SDW) QCP, described by the Hertz-Millis theory^{14,15}. A proposed global phase diagram¹⁶⁻¹⁹ makes this connection via the tuning of the quantum fluctuations in the local-moment magnetism. Besides the HF metals, it is also interesting to know whether a similar global phase diagram can be realized in Kondo insulators (KIs), where the chemical potential is inside the Kondo hybridization gap when the electron filling is commensurate. The KIs are nontrivial band insulators because the band gap originates from strong electron-correlation effects. A Kondo-destruction

transition is expected to accompany the closure of the band gap. The question that remains open is whether the local moments immediately order or form a different type of magnetic states, such as spin liquid or valence bond solid (VBS), when the Kondo destruction takes place.

Recent years have seen extensive studies about the effect of a fine spin-orbit coupling (SOC) on the electronic bands. In topological insulators (TIs), the bulk band gap opens due to a nonzero SOC, and there exist gapless surface states. The nontrivial topology of the bandstructure is protected by the time reversal symmetry (TRS). Even for a system with broken TRS, the conservation of combination of TRS and translational symmetry can give rise to a topological antiferromagnetic insulator (T-AFMI).²⁰ In general, these TIs and TAFIs can be tuned to topologically trivial insulators via topological quantum phase transitions. But how the strong electron correlations influence the properties of these symmetry dictated topological phases and related phase transitions is still under active discussion.

The SOC also has important effects in HF materials¹⁹. For example, the SOC can produce a topologically nontrivial bandstructure and induce exotic Kondo physics.^{21,22} it may give rise to a topological Kondo insulator (TKI),²³ which has been invoked to understand the resistivity plateau of the heavy-fermion SmB₆ at low temperatures.²⁴

From a more general perspective, SOC provides an additional tuning parameter enriching the global phase diagram of HF systems^{19,25}. Whether and how the topological nontrivial quantum phases can emerge in this phase diagram is a timely issue. Recent studies have advanced a Weyl-Kondo semimetal phase²⁶. Experimental evidence has come from the new heavy fermion compound Ce₃Bi₄Pd₃, which display thermodynamic²⁷ and zero-

field Hall transport²⁸ properties that provide evidence for the salient features of the Weyl-Kondo semimetal. These measurements respectively probe a linearly dispersing electronic excitations with a velocity that is renormalized by several orders of magnitude and singularities in the Berry-curvature distribution.

This type of theoretical studies are also of interest for a Kondo lattice model defined on a honeycomb lattice,²⁹ which readily accommodates the SOC³⁰. In the dilute-carrier limit, this model supports a nontrivial Dirac-Kondo semimetal (DKSM) phase, which can be tuned to a TKI by increasing SOC.³¹ In Ref. 29, it was shown that, at half-filling, increasing the Kondo coupling induces a direct transition from a TI to a KI. A related model, with the conduction-electron part of the Hamiltonian described by a Haldane model³² on the honeycomb lattice, was subsequently studied.³³

Here we investigate the global phase diagram of a spin-orbit-coupled Kondo lattice model on the honeycomb lattice at half-filling. We show that the competing interactions in this model give rise to a very rich phase diagram containing a TI, a KI, and two AFM phases. We focus on discussing the influence of magnetic frustration on the phase diagram. In the TI, the local moments develop a VBS order. In the two AFM phases, the moments are ordered, respectively, in the plane of the honeycomb lattice (denoted as AFM_{xy}) and perpendicular to the plane (AFM_z). Particularly in the AFM_z phase, the conduction electrons may have a topologically nontrivial bandstructure, although the TRS is explicitly broken. This T-AFM_z state connects to the trivial AFM_z phase via a topological phase transition as the SOC is reduced.

The remainder of the paper is organized as follows. We start by introducing the model and our theoretical procedure in Sec.II. In Sec.III we discuss the magnetic phase diagram of the Heisenberg model for the local moments. Next we obtain the global phase diagram of the full model in Sec. IV. In Sec V we examine the nature of the conduction-electron bandstructures in the AFM states, with a focus on their topological characters. We discuss the implications of our results in Sec. VI.

II. MODEL AND METHOD

The model we consider here is defined on an effective double-layer honeycomb lattice. The top layer contains conduction electrons realizing the Kane-Mele Hamiltonian³⁰. The conduction electrons are Kondo coupled to (*i.e.*, experiencing an AF exchange coupling J_K with) the localized magnetic moments in the bottom layer. The local moments interact among themselves through direct exchange interaction as well as the conduction electron mediated RKKY interaction; this interaction is described by a simple J_1 - J_2 model. Both the conduction bands and the localized bands are half-filled. This Kondo-lattice Hamiltonian takes the following form on the honeycomb

lattice:

$$H = t \sum_{\langle ij \rangle \sigma} c_{i\sigma}^\dagger c_{j\sigma} + i\lambda_{\text{so}} \sum_{\langle\langle ij \rangle\rangle \sigma \sigma'} v_{ij} c_{i\sigma}^\dagger \sigma_{\sigma\sigma'}^z c_{j\sigma'} + J_K \sum_i \vec{s}_i \cdot \vec{S}_i + J_1 \sum_{\langle ij \rangle} \vec{S}_i \cdot \vec{S}_j + J_2 \sum_{\langle\langle ij \rangle\rangle} \vec{S}_i \cdot \vec{S}_j, (1)$$

where $c_{i\sigma}^\dagger$ creates a conduction electron at site i with spin index σ . t is the hopping parameter between the nearest neighboring (NN) sites, and λ_{so} is the strength of the SOC between next-nearest neighboring (NNN) sites. $v_{ij} = \pm 1$, depending on the direction of the NNN hopping. $\vec{s}_i = c_{i\sigma}^\dagger \vec{\sigma}_{\sigma\sigma'} c_{i\sigma'}$, is the spin operator of the conduction electrons at site i with $\vec{\sigma} = \sigma^x, \sigma^y, \sigma^z$ being the pauli matrices. \vec{S}_i refers to the spin operator of the local moments with spin size $S = 1/2$. In the model we considered here, J_K , J_1 , and J_2 are all AF. By incorporating the Heisenberg interactions, the Kondo-lattice model we study readily captures the effect of geometrical frustration. In addition, instead of treating the Kondo screening and magnetic order in terms of the longitudinal and transverse components of the Kondo-exchange interactions^{33,34,36}, we will treat both effects in terms of interactions that are spin-rotationally invariant; this will turn out to be important in mapping out the global phase diagram.

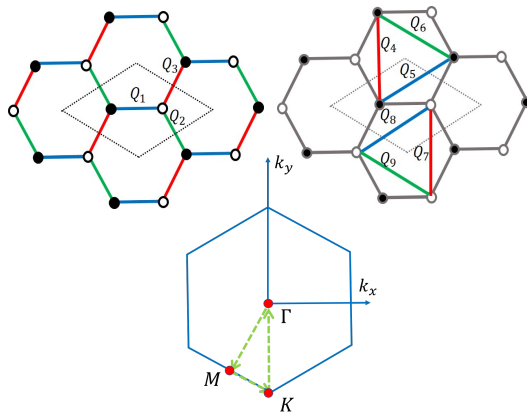


FIG. 1. Top panels: Definition of nearest neighboring and next nearest neighboring valence bond fields Q_{ij} . Filled and empty circles denote the two sublattices A and B, respectively. Different bond directions are labeled by different colors. Bottom panel: First Brillouin zone corresponding to the two-sublattice unit cell.

We use the spinon representation for \vec{S}_i , *i.e.*, by rewriting $\vec{S}_i = f_{i\sigma}^\dagger \vec{\sigma}_{\sigma\sigma'} f_{i\sigma'}$ along with the constraint $\sum_{\sigma} f_{i\sigma}^\dagger f_{i\sigma} = 1$, where $f_{i\sigma}^\dagger$ is the spinon operator. The constraint is enforced by introducing the Lagrange multiplier term $\sum_i \lambda_i (\sum_{\sigma} f_{i\sigma}^\dagger f_{i\sigma} - 1)$ in the Hamiltonian. In order to study both the non-magnetic and magnetic phases, we decouple the Heisenberg Hamiltonian into two

channels:

$$\begin{aligned}
& J\mathbf{S}_i \cdot \mathbf{S}_j \\
&= xJ\mathbf{S}_i \cdot \mathbf{S}_j + (1-x)J\mathbf{S}_i \cdot \mathbf{S}_j \\
&\simeq x \left(\frac{J}{2}|Q_{ij}|^2 - \frac{J}{2}Q_{ij}^* f_{i\alpha}^\dagger f_{j\alpha} - \frac{J}{2}Q_{ij} f_{j\alpha}^\dagger f_{i\alpha} \right) \\
&+ (1-x)(-J\mathbf{M}_i \cdot \mathbf{M}_j + J\mathbf{M}_j \cdot \mathbf{S}_i + J\mathbf{M}_i \cdot \mathbf{S}_j) \quad (2)
\end{aligned}$$

Here x is a parameter that is introduced in keeping with the generalized procedure of Hubbard-Stratonovich decouplings and will be fixed to conveniently describe the effect of quantum fluctuations. The corresponding valence bond (VB) parameter Q_{ij} and sublattice magnetization \mathbf{M}_i are $Q_{ij} = \langle \sum_\alpha f_{i\alpha}^\dagger f_{j\alpha} \rangle$ and $\mathbf{M}_i = \langle \mathbf{S}_i \rangle$, respectively. Throughout this paper, we consider the two-site unit cell thus excluding any states that breaks lattice translation symmetry. Under this construction, there are 3 independent VB mean fields Q_i , $i = 1, 2, 3$, for the NN bonds and 6 independent VB mean fields Q_i , $i = 4, 5, \dots, 9$, for the NNN bonds. They are illustrated in Fig. 1. We consider only AF exchange interactions, $J_1 > 0$ and $J_2 > 0$, and will thus only take into account AF order with $\mathbf{M} = \mathbf{M}_{i \in A} = -\mathbf{M}_{i \in B}$.

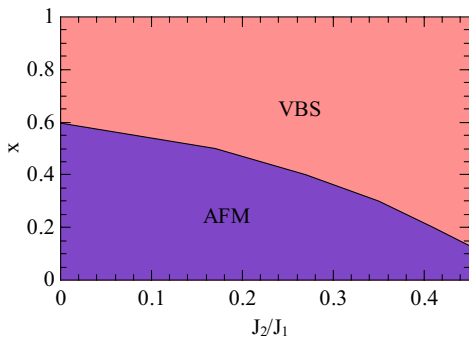


FIG. 2. Ground-state phase diagram of the J_1 - J_2 Hamiltonian for the local moments in the x - J_2/J_1 plane. A NN VBS and an AFM state are stabilized in the parameter regime shown.

To take into account the Kondo hybridization and the possible magnetic order on an equal footing, we follow the treatment of the Heisenberg interaction as outlined in Eq. 2 and decouple the Kondo interaction as follows:

$$\begin{aligned}
& J_K \mathbf{S} \cdot \mathbf{s} \\
&\simeq y \left(\frac{J_K}{2}|b|^2 - \frac{J_K}{2}b f_{i\alpha}^\dagger c_{i\alpha} - \frac{J_K}{2}b^* c_{i\alpha}^\dagger f_{i\alpha} \right) \\
&+ (1-y)(-J_K \mathbf{M}_i \cdot \mathbf{m}_i + J_K \mathbf{S}_i \cdot \mathbf{m}_i + J_K \mathbf{s}_i \cdot \mathbf{M}_i) \quad (3)
\end{aligned}$$

Here we have introduced the mean-field parameter for the Kondo hybridization, $b = \langle \sum_\alpha c_{i\alpha}^\dagger f_{i\alpha} \rangle$, and the conduction electron magnetization: $\mathbf{m}_i = \langle \mathbf{s}_i \rangle$. For nonzero b , the conduction band will Kondo hybridize with the local moments and the system at half-filling is a KI. On the other hand, when b is zero and \mathbf{M} is nonzero, magnetization ($\mathbf{m} \neq 0$) on the conduction electron band will

be induced by the Kondo coupling, and various AF orders can be stabilized depending on the strength of the SOC. Just like the parameter x of Eq. 2 is chosen so that a saddle-point treatment captures the quantum fluctuations in the form of spin-singlet bond parameters¹⁸, the parameter y will be specified according to the criterion that the treatment at the same level describes the quantum fluctuations in the form of Kondo-insulator state (see below).

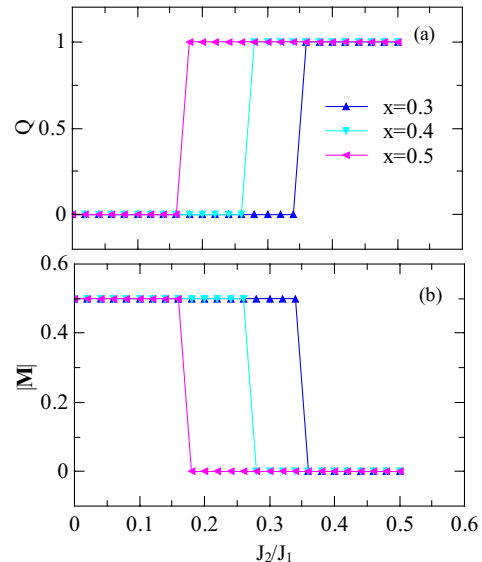


FIG. 3. Evolution of the VBS order parameter Q [in (a)] and the AFM order parameter M [in (b)] as a function of J_2/J_1 for $x = 0.3, 0.4, 0.5$.

III. PHASE DIAGRAM OF THE HEISENBERG MODEL FOR THE LOCAL MOMENTS

Because of the complexity of the full Hamiltonian, we start by setting $J_K = 0$ and discuss the possible ground-state phases of the J_1 - J_2 Heisenberg model for the local moments. By treating the problem at the saddle-point level in Eq. (2), we obtain the phase diagram in the x - J_2/J_1 plane shown in Fig.2. Here the x -dependence is studied in the same spirit as that of Ref. 18 for the Shastry-Sutherland lattice. In the parameter regime explored, an AF ordered phase (labeled as “AFM” in the figure) and a valence bond solid (VBS) phase are stabilized. The AF order stabilized is the two-sublattice Néel order on the honeycomb lattice, and the VBS order refers to covering of dimer singlets with $|Q_i| = Q \neq 0$ for one out of the three NN bonds (e.g. $Q_1 \neq 0, Q_2 = Q_3 = 0$) and $|Q_i| = 0$ for all the NNN bonds. This VBS state spontaneously breaks the C_3 rotational symmetry of the lattice. We thus define the order parameter for VBS state to be $Q = |\sum_{j=1,2,3} Q_j e^{i(2\pi j/3)}|$.

In Fig. 3 we plot the evolution of VBS and AF order parameters Q and M as a function of J_2/J_1 . A direct first-order transition (signaled by the mid-point of the jump of the order parameters) between these two phases is observed for $x \lesssim 0.6$. For the sake of understanding the global phase diagram of the full Kondo-Heisenberg model, we limit our discussion to $J_2/J_1 < 1$, where only the NN VBS is relevant. A different decoupling scheme approach was used to study this model³⁵ found results that are, in the parameter regime of overlap, consistent with ours. To fix the parameter x , we compare our results with those about the $J_1 - J_2$ model derived from previous numerical studies. DMRG studies³⁷ found that the AFM state is stabilized for $J_2/J_1 < 0.22$, and VBS exists for $J_2/J_1 > 0.35$, while in between the nature of the ground states are still under debate. In this parameter regime, the DMRG calculations suggest a plaquette resonating valence bond (RVB) state,³⁷ while other methods implicate possibly spin liquids.³⁸ In light of these numerical results, we take $x = 0.4$ in our calculations. This leads to a direct transition from AFM to VBS at $J_2/J_1 \simeq 0.27$, close to the values of phase boundaries of these two phases determined by other numerical methods.

IV. GLOBAL PHASE DIAGRAM OF THE KONDO-LATTICE MODEL

We now turn to the global phase diagram of the full model by turning on the Kondo coupling. For definiteness, we set $J_1 = 1$ and consider $t = 1$ and $\lambda_{so} = 0.4$. As prescribed in the previous section, we take $x = 0.4$. Similar considerations for y require that its value allows for quantum fluctuations in the form of Kondo-singlet formation. This has guided us to take $y = 0.7$ (see below). The corresponding phase diagram as a function of J_K and the frustration parameter J_2/J_1 is shown in Fig. 4.

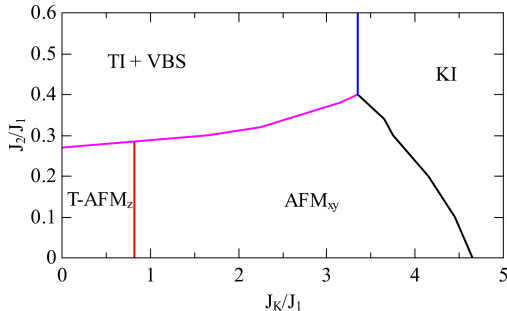


FIG. 4. Global phase diagram at $T = 0$ from the saddle-point calculations with $x = 0.4$, $y = 0.7$. The ground states include the valence-bond solid (VBS) and Kondo insulator (KI), as well as two antiferromagnetic orders, T-AFM _{z} and AFM _{xy} , as described in Sec. V.

In our calculation, the phase boundaries are determined by sweeping J_K while along multiple horizontal

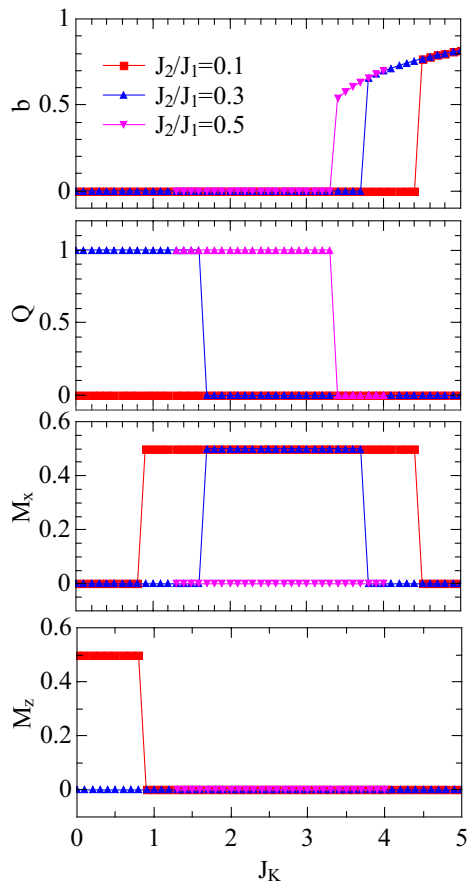


FIG. 5. Evolution of the parameters b , Q , M_x and M_z as a function of J_K for different ratio of J_2/J_1 .

cuts for several fixed J_2/J_1 values, as shown in Fig. 5. For small J_K and large J_2/J_1 , the local moments and the conduction electrons are still effectively decoupled. The conduction electrons form a TI for finite SOC, and the local moments are in the VBS ground state as discussed in the previous section. When both J_K and J_2/J_1 are small, the ground state is AFM. Due to the Kondo coupling, finite magnetization \mathbf{m} is induced for the conduction electrons. This opens a spin density wave (SDW) gap in the conduction band, and therefore the ground state of the system is an AFM insulator. The SOC couples the rotational symmetry in the spin space to the one in real space. As a consequence, the ordered moments in the AFM phase can be either along the z direction (AFM _{z}) or in the x - y plane (AFM _{xy}). For finite SOC, these two AFM states have different energies, which can be tuned by J_K . As shown in the phase diagram, the AFM phase contains two ordered states, the AFM _{z} and AFM _{xy} . They are separated by a spin reorientation transition at $J_K/J_1 \approx 0.8$. For the value of SOC taken, the AFM state is topologically nontrivial, and is hence denoted as T-AFM _{z} state. The nature of this state and the associated topological phase transition is discussed in detail in the next section.

For sufficiently large J_K , the Kondo hybridization b is nonzero (see Fig.5(a)), and the ground state is a KI. Note that for finite SOC, this KI does not have a topological nontrivial edge state, as a consequence of the topological no-go theorem^{29,39,40}. In our calculation at the saddle-point level, the KI exists for $y \geq 0.6$; this provides the basis for taking $y = 0.7$, as noted earlier. Going beyond the saddle-point level, the dynamical effects of the Kondo coupling will appear, and we will expect the KI phase to arise for other choices of y .

Several remarks are in order. The phase diagram, Fig. 4, has a similar profile of the global phase diagram for the Kondo insulating systems^{25,41}. However, the presence of SOC has enriched the phase diagram. In the AF state, the ordered moment may lie either within the plane or be perpendicular to it. These two states have very different topological properties. We now turn to a detailed discussion of this last point.

V. TOPOLOGICAL PROPERTIES OF THE AFM STATES

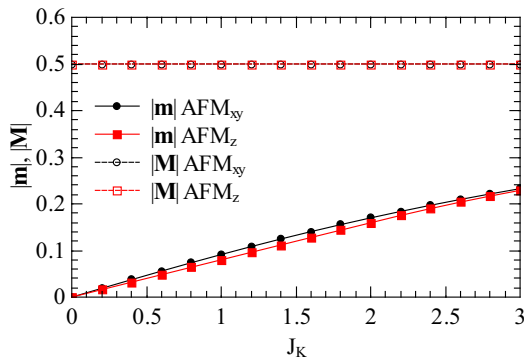


FIG. 6. The conduction electron magnetization for the AFM_{xy} and AFM_z states at $\lambda_{so} = 0.1$.

In this section we discuss the properties of the AFM_{xy}

and AFM_z states, in particular to address their topological nature. For a clear discussion, we fix $t = 1$, $J_1 = 1$, and $J_2 = 0$. Since the Kondo hybridization is not essential to the nature of the AFM states, in this section we simply the discussion by setting $y = 0$.

We start by defining the order parameters of the two states:

$$M_x = \langle S_{f,A}^x \rangle = -\langle S_{f,B}^x \rangle, \quad (4)$$

$$M_z = \langle S_{f,A}^z \rangle = -\langle S_{f,B}^z \rangle, \quad (5)$$

$$m_x = -\langle s_{c,A}^x \rangle = \langle s_{c,B}^x \rangle, \quad (6)$$

$$m_z = -\langle s_{c,A}^z \rangle = \langle s_{c,B}^z \rangle. \quad (7)$$

Note that for AFM_{xy} state we set $M_x = m_y = 0$ without losing generality. In Fig.(6) we plot the evolution of these AFM order parameters with J_K for a representative value of SOC $\lambda_{so} = 0.1$. Due to the large J_1 value we take, the sublattice magnetizations of the local moments are already saturated to 0.5. Therefore, at the saddle-point level, they serve as effective (staggered) magnetic fields to the conduction electrons. The Kondo coupling then induces finite sublattice magnetizations for the conduction electrons, and they increase linearly with J_K for small J_K values. But m_x is generically different from m_z . This is important for the stabilization of the states.

We then discuss the energy competition between the AFM_{xy} and AFM_z states. The conduction electron part of the mean-field Hamiltonian reads:

$$H_c = \begin{pmatrix} c_{A\uparrow}^\dagger & c_{A\downarrow}^\dagger & c_{B\uparrow}^\dagger & c_{B\downarrow}^\dagger \end{pmatrix}^T h_{MF} \begin{pmatrix} c_{A\uparrow} \\ c_{A\downarrow} \\ c_{B\uparrow} \\ c_{B\downarrow} \end{pmatrix} \quad (8)$$

with

$$h_{MF} = \begin{pmatrix} \Lambda(k) & J_K M_x/2 & \epsilon(k) & \\ J_K M_x/2 & -\Lambda(k) & & \epsilon(k) \\ \epsilon^*(k) & & -\Lambda(k) & -J_K M_x/2 \\ & \epsilon^*(k) & -J_K M_x/2 & \Lambda(k) \end{pmatrix} \quad (9)$$

for the AFM_{xy} state and

$$h_{MF} = \begin{pmatrix} \Lambda(k) + J_K M_z/2 & & \epsilon(k) & \\ & -\Lambda(k) - J_K M_z/2 & & \epsilon(k) \\ \epsilon^*(k) & & -\Lambda(k) - J_K M_z/2 & \\ & \epsilon^*(k) & & \Lambda(k) + J_K M_z/2 \end{pmatrix} \quad (10)$$

for the AFM_z state. Here $\Lambda(k) = 2\lambda_{so}(\sin(k \cdot a_1) - \sin(k \cdot a_2) - \sin(k \cdot (a_1 - a_2)))$, $\epsilon(k) = t_1(1 + e^{-ik \cdot a_1} + e^{-ik \cdot a_2})$, $\epsilon^*(k)$ is the complex conjugate of $\epsilon(k)$, and $a_1 = (\sqrt{3}/2, 1/2)$, $a_2 = (\sqrt{3}/2, -1/2)$ are the primitive vectors. For both states the eigenvalues

are doubly degenerate.

$$E_{\pm,xy}^c(k) = \pm \sqrt{\Lambda(k)^2 + (J_K M_x/2)^2 + |\epsilon(k)|^2} \quad (11)$$

$$E_{\pm,z}^c(k) = \pm \sqrt{(\Lambda(k) + J_K M_z/2)^2 + |\epsilon(k)|^2} \quad (12)$$

The eigenenergies of the spinon band can be obtained

in a similar way:

$$E_{\pm,xy}^f(k) = \pm \frac{1}{2}(3J_1 M_x + J_K m_x), \quad (13)$$

$$E_{\pm,z}^f(k) = \pm \frac{1}{2}(3J_1 M_z + J_K m_z). \quad (14)$$

The expression of total energy for either state is then

$$E_{tot} = 2 \frac{1}{N_k} \sum_k E_-^c(k) + 2 \frac{1}{N_k} \sum_k E_-^f(k) + 3J_1 |\mathbf{M}|^2 + 2J_K (\mathbf{M} \cdot \mathbf{m}). \quad (15)$$

The first line of the above expression comes from filling the bands up to the Fermi energy (which is fixed to be zero here). The second line is the constant term in the mean-field decomposition. The factor of 2 in the k summation is to take into account the double degeneracy of the energies. N_k refers to the number of k points in the first Brillouin zone.

By comparing the expressions of $E_-^c(k)$ in Eqns. (11) and (12), we find that adding a small M_x is to increase the size of the gap at both of the two (inequivalent) Dirac points, thereby pushing the states further away from the Fermi-energy. While adding a small M_z is to enlarge the gap at one Dirac point but reduce the gap size at the other one. Therefore, an AFM_{xy} state is more favorable than the AFM_z state in lowering the energy of conduction electrons $\sum_k E_-^c(k)$.

On the other hand, from Eqns.(13)-(15), we see that the overall effect of adding a magnetization of the conduction band, \mathbf{m} , is to increase the total energy E_{tot} (the main energy increase comes from the $2J_K(\mathbf{M} \cdot \mathbf{m})$ term). Because $|m_z| < |m_x|$ from the self consistent solution, as shown in Fig. 6, the energy increase of the AFM_z state is smaller than that in the AFM_{xy} state.

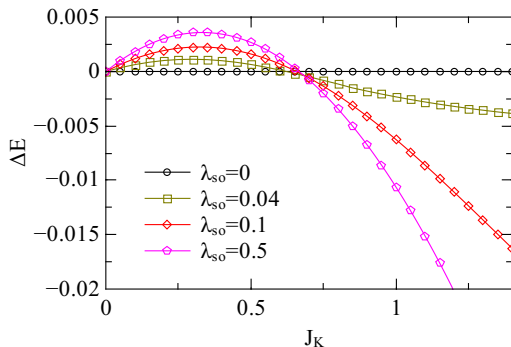


FIG. 7. The energy difference between AFM_z and AFM_{xy} states as a function of J_K for various values of spin-orbital coupling λ_{so} .

With increasing J_K the above two effects from the magnetic orders compete, resulting in different magnetic ground states as shown in Fig. 4. This analysis is further supported by our self-consistent mean-field calculation. In Fig. 7 we plot the energy difference between these two states $\Delta E = E_{xy} - E_z$ as a function of J_K at several λ_{so}

values. In the absence of SOC, the model has the spin SU(2) symmetry, and the AFM_z and AFM_{xy} states are degenerate with $\Delta E = 0$. For finite λ_{so} , at small J_K values, the energy gain from the $\sum_k E_-^c(k)$ term dominates, $\Delta E > 0$, and the ground state is an AFM_z state. With increasing J_K , the contribution from the $2J_K(\mathbf{M} \cdot \mathbf{m})$ term is more important. ΔE crosses zero to be negative, and the AFM_{xy} state is eventually energetically favorable for large J_K .

Next we discuss the topological nature of the AFM_z and AFM_{xy} state. In the absence of Kondo coupling J_K , the conduction electrons form a TI, which is protected by the TRS. Their the left- and right-moving edge states connecting the conduction and valence bands are respectively coupled to up and down spin flavors (eigenstates of the S^z operator) as the consequence of SOC, and these two spin polarized edge states do not mix.

Once the TRS is broken by the AFM order, generically, topologically nontrivial edge states are no longer guaranteed. However, in the AFM_z state, the structure of the Hamiltonian for the conduction electrons is as same as that in a TI. This is clearly shown in Eq. (10): the effect of magnetic order is only to shift $\Lambda(k)$ to $\Lambda(k) + J_K M_z/2$. In particular, the spin-up and spin-down sectors still do not mix each other. Therefore, the two spin polarized edge states are still well defined as in the TI, and the system is topologically nontrivial though without the protection of TRS. Note that the above analysis is based on assuming $J_K M_z \ll \Lambda(k)$, where the bulk gap between the conduction and valence bands is finite. For $J_K M_z > 6\sqrt{3}\lambda_{so}/(1-y)$, the bulk gap closes at one of the inequivalent Dirac points and the system is driven to a topologically trivial phase via a topological phase transition.²⁹ We also note that a similar AFM_z state arises in a Kondo lattice model without SOC but with a Haldane coupling, as analyzed in Ref. 33.

For the AFM_{xy} state, we can examine the Hamiltonian for the conduction electrons in a similar way. As shown in Eq. (9), the transverse magnetic order M_x mixes the spin-up and spin-down sectors. As a result, a finite hybridization gap opens between the two edge states making the system topologically trivial.

To support the above analysis, we perform calculations of the energy spectrum of the conduction electrons in the AFM_z and AFM_{xy} states, as shown in Eq.(9) and Eq.(10), on a finite slab of size $L_x \times L_y$, with $L_x = 200$ and $L_y = 40$. The boundary condition is chosen to be periodic along the x direction and open and zig-zag-type along the y direction. In Fig. 8 we show the plots of the energy spectra with three different set of parameters: (a) $\lambda_{so} = 0.01$, $J_K = 0.4$, $M_z = 0.5$, (b) $\lambda_{so} = 0.0$, $J_K = 0.4$, $M_z = 0.5$, and (c) $\lambda_{so} = 0.0$, $J_K = 0.8$, $M_x = 0.5$, which respectively correspond to the topologically trivial AFM_z state, topological AFM_z insulator, and AFM_{xy} state. As clearly seen, the gapless edge states only exist for parameter set (b), where the system is in the topological AFM_z state. Note that in this state, the spectrum is asymmetric with respect to the Brillouin zone boundary

($k_x = \pi$), reflecting the explicit breaking of TRS. Based on our analysis and numerical calculations, we construct a phase diagram, shown in Fig. 9, to illustrate the competition of these AFM states. As expected, the AFM_z state is stabilized for $J_K \lesssim 0.7$, and is topological for $J_K < 12\sqrt{3}\lambda_{so}$ (above the red line).

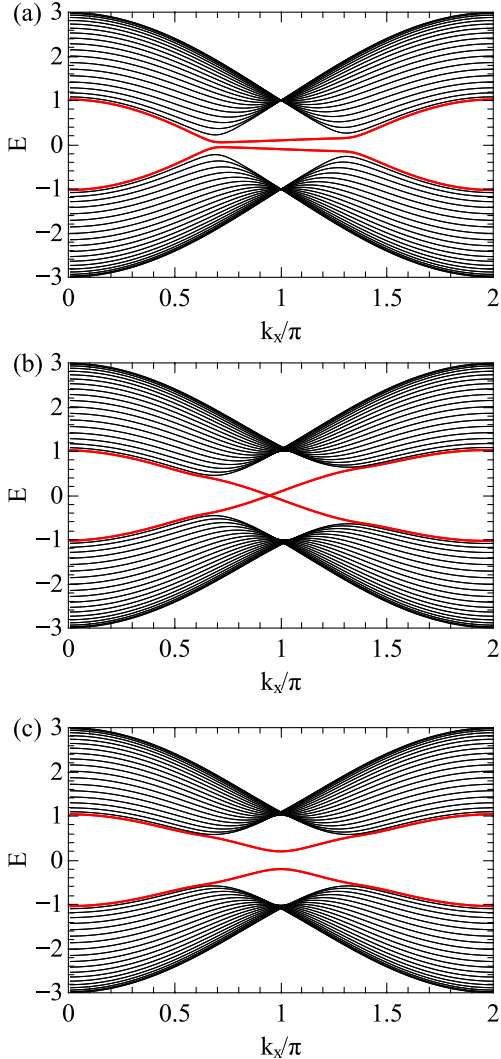


FIG. 8. Energy spectra of the trivial AFM_z state [in (a)], the topological AFM_z insulator [in (b)], and the AFM_{xy} state [in (c)] from finite slab calculations. Black lines denote the bulk states and red lines denote edge states. The topological AFM_z state is characterized by the gapless edge states. See text for detailed information on the parameters.

VI. DISCUSSION AND CONCLUSION

We have discussed the properties of various phases in the ground-state phase diagram of the spin-orbit-coupled Kondo lattice model on the honeycomb lattice at half filling. We have shown how the competition of SOC,

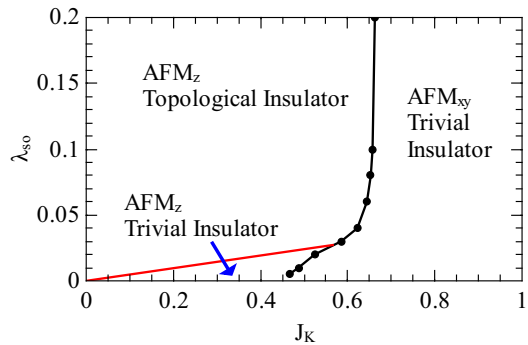


FIG. 9. Phase diagram in the λ_{so} - J_K plane showing the competition of various AFM states. The red line denotes a topological phase transition between the topological trivial and topological nontrivial AFM_z states, and the black curve gives the boundary between the AFM_z and AFM_{xy} states. These two states become equivalent in the limit of $\lambda_{so} \rightarrow 0$.

Kondo interaction, and magnetic frustration stabilizes these phases. For example, in the AFM phase the moments can order either along the z -direction or within the x - y plane. In our model, the AFM order is driven by the RKKY interaction, and the competition of SOC and Kondo interaction dictates the direction of the ordered magnetic moments.

Throughout this work, we have discussed the phase diagram of the model at half filling. The phase diagram away from half-filling is also an interesting problem. We expect that the competition between the AFM_z and AFM_{xy} states persists at generic fillings, but the topological feature will not. Another interesting filling would be the dilute-carrier limit, where a DKSM exists, and can be tuned to a TKI by increasing SOC.³¹

In this work we have considered a particular type of SOC, which is inherent in the bandstructure of the itinerant electrons. In real materials, there are also SOC terms that involve the magnetic ions. Such couplings will lead to models beyond the current work, and may further enrich the global phase diagram.

In conclusion, we have investigated the ground-state phase diagram of a spin-orbit coupled Kondo-lattice model at half-filling. The combination of SOC, Kondo and RKKY interactions produces various quantum phases, including a Kondo insulator, a topological insulator with VBS spin correlations, and two AFM phases. Depending on the strength of SOC, the magnetic moments in the AFM phase can be either ordered perpendicular to or in the x - y plane. We further show that the z -AFM state is topologically nontrivial for strong and moderate SOC, and can be tuned to a topologically trivial one via a topological phase transition by varying either the SOC or the Kondo coupling. Our results shed new light on the global phase diagram of heavy fermion materials.

ACKNOWLEDGEMENTS

We thank W. Ding, P. Goswami, S. E. Grefe, H.-H. Lai, Y. Liu, S. Paschen, J. H. Pixley, T. Xiang, and G. M. Zhang for useful discussions. Work at Renmin University was supported by the Ministry of Science and Technology of China, National Program on Key Research Project Grant number 2016YFA0300504, the National

Science Foundation of China Grant number 11674392 and the Research Funds of Renmin University of China Grant number 18XNNG24. Work at Rice was in part supported by the NSF Grant DMR-1611392 and the Robert A. Welch Foundation Grant C-1411. Q.S. acknowledges the hospitality and support by a Ulam Scholarship from the Center for Nonlinear Studies at Los Alamos National Laboratory.

-
- * rong.yu@ruc.edu.cn
† qmsi@rice.edu
- ¹ Special issue on Quantum Phase Transitions, *J. Low Temp. Phys.* **161**, 1 (2010).
 - ² S. Sachdev, *Quantum Phase Transitions* (Cambridge University Press, Cambridge, 2011), 2nd ed.
 - ³ Q. Si and F. Steglich, *Science* **329**, 1161C1166 (2010).
 - ⁴ P. Gegenwart, Q. Si, and F. Steglich *Nat. Phys.* **4**, 186 - 197 (2008).
 - ⁵ H. von Löhneysen, A. Rosch, M. Vojta, and P. Wölfle, *Rev. Mod. Phys.* **79**, 1015 (2007).
 - ⁶ H. Tsunetsugu, M. Sigrist, and K. Ueda, *Rev. Mod. Phys.* **69**, 809 (1997).
 - ⁷ A. C. Hewson, *The Kondo Problem to Heavy Fermions*, Cambridge Univ. Press, Cambridge, England (1993).
 - ⁸ S. Doniach, *Physica B+C* **91**, 231-234 (1977).
 - ⁹ J. Custers, *et al.*, *Nature* **424**, 524-527 (2003).
 - ¹⁰ A. Schröder *et al.*, *Nature* **407**, 351 (2000).
 - ¹¹ S. Paschen, T. Luhmann, S. Wirth, P. Gegenwart, O. Trovarelli, C. Geibel, F. Steglich, P. Coleman, and Q. Si, *Nature* **432**, 881 (2004).
 - ¹² Q. Si, S. Rabello, K. Ingersent, and J. L. Smith, *Nature* **413**, 804 (2001).
 - ¹³ P. Coleman, C. Pépin, Q. Si, and R. Ramazashvili, *J. Phys.: Condens. Matter* **13**, R723-R738 (2001).
 - ¹⁴ J. A. Hertz, *Phys. Rev. B* **14**, 1165-1184 (1976).
 - ¹⁵ A. J. Millis, *Phys. Rev. B* **48**, 7183-7196 (1993).
 - ¹⁶ Q. Si, *Physica B* **378-380**, 23-27 (2006).
 - ¹⁷ Q. Si, *Phys. Stat. Solid. B* **247**, 476-484 (2010).
 - ¹⁸ J. H. Pixley, R. Yu, and Q. Si, *Phys. Rev. Lett.* **113**, 176402 (2014).
 - ¹⁹ Q. Si and S. Paschen, *Phys. Stat. Solid. B* **250**, 425-438 (2013).
 - ²⁰ R. S. K. Mong, A. M. Essin, and J. E. Moore, *Phys. Rev. B* **81**, 245209 (2010).
 - ²¹ S. Nakatsuji *et al.*, *Phys. Rev. Lett.* **96**, 087204 (2006).
 - ²² G. Chen, *Phys. Rev. B* **94**, 205107 (2016).
 - ²³ M. Dzero, K. Sun, V. Galitski, and P. Coleman, *Phys. Rev. Lett.* **104**, 106408 (2010).
 - ²⁴ A. Barla *et al.*, *Phys. Rev. Lett.* **94**, 166401 (2005).
 - ²⁵ S. Yamamoto and Q. Si, *J. Low Temp. Phys.* **161**, 233-262 (2010).
 - ²⁶ H.-H. Lai, S. E. Grefe, S. Paschen, and Q. Si, *PNAS* **115**, 93 (2018).
 - ²⁷ S. Dzsaber *et al.*, *Phys. Rev. Lett.* **118**, 246601 (2017).
 - ²⁸ S. Dzsaber *et al.* arXiv:1811.02819.
 - ²⁹ X.-Y. Feng, C.-H. Chung, J. Dai, and Q. Si, *Phys. Rev. Lett.* **111**, 016402 (2013).
 - ³⁰ C. L. Kane and E. J. Mele, *Phys. Rev. Lett.* **95**, 226801 (2005).
 - ³¹ X.-Y. Feng, H. Zhong, J. Dai, and Q. Si, arXiv:1605.02380 (2016).
 - ³² F. D. M. Haldane, *Phys. Rev. Lett.* **61**, 2015 (1988).
 - ³³ Y. Zhong, Y.-F. Wang, Y.-Q. Wang, and H.-G. Luo, *Phys. Rev. B* **87**, 035128 (2013).
 - ³⁴ C. Lacroix and M. Cyrot, *Phys. Rev. B* **20**, 1969 (1979).
 - ³⁵ H. Li, H.-F. Song, and Y. Liu, *EuroPhys. Lett.* **116**, 37005 (2016).
 - ³⁶ H. Li, Y. Liu, G.-M. Zhang, and L. Yu, *J. Phys.: Condens. Matter* **27**, 425601 (2015).
 - ³⁷ R. Ganesh, J. van den Brink, and S. Nishimoto, *Phys. Rev. Lett.* **110**, 127203 (2013).
 - ³⁸ B. K. Clark, D. A. Abanin, S. L. Sondhi, *Phys. Rev. Lett.* **107**, 087204(2011).
 - ³⁹ M. Z. Hasan and C. L. Kane, *Rev. Mod. Phys.* **82**, 3045 (2010).
 - ⁴⁰ X.-L. Qi and S.-C. Zhang, *Rev. Mod. Phys.* **83**, 1057C1110 (2011).
 - ⁴¹ J. H. Pixley, R. Yu, S. Paschen, and Q. Si, *Phys. Rev. B* **98**, 085110 (2018).